VIP Bone Repair Very Important Paper

DOI: 10.1002/ange.201305759

Bone-Crack Detection, Targeting, and Repair Using Ion Gradients**

Vinita Yadav, Jonathan D. Freedman, Mark Grinstaff, and Ayusman Sen**

Self-powered nanomotors and pumps are increasingly being explored for biological applications given the advances in basic motor design and functionality over the last decade.[1] Such autonomous devices, requiring no external power supply, offer a broad range of potential biomedical applications ranging from targeted drug delivery to minimally invasive surgeries. Ion gradients can cause diffusiophoretic transport of fluid and particles and provide one method for directing movement towards specific targets. We describe here a strategy based on a biological synthetic hybrid micropump for the detection of bone lesions by utilizing the damaged matrix itself as both the trigger and the fuel. A crack in a high-mineral-content material, such as bone, generates ion-gradient-driven electric fields, which can be utilized for active targeting and treatment. The role of electric fields and ensuing electrophoresis as a mechanism for the directional movement of motile cells has also recently been illustrated.[2] Our strategy is also applicable to synthetic surfaces with equal efficiency.

Our approach complements but is orthogonal to current methods that promote healing by delivery of a therapeutic agent to the bone through passive diffusion.[3] These current clinical treatments include systemic antiresorptive (bisphosphonates[4]) or anabolic therapies (parathyroid hormone therapy[5]), which are useful for general increase in mineralization and bone strength in patients. However, since bone diseases like osteoporosis vary in degree of degeneration at different skeletal sites, fractures of vulnerable areas like the hip, spine, and wrist are common even with preventative therapies.[6] Consequently, a variety of new targeting strategies to increase drug delivery to the bone are currently being investigated and include, for example environmentally sensitive cleavable linker systems, and fusion proteins or nanoparticles with bone-targeting moieties.[7] While these treatments enhance the specificity to bone, mechanisms for active delivery of agents to target sites that are most at risk for fracture or of active degeneration remain elusive and are highly desired. Described below is the active detection of ex vivo human bone cracks by using charged quantum dots and a strategy for repair that is based on the phenomenon of diffusiophoretic motion.

Our approach is based on the generation of ion gradients from freshly exposed mineral surfaces, which results in a local electric field that can be exploited for targeting and treatment. Bone is a composite material that supports load. It is composed of collagen and a mineral matrix most closely resembling hydroxyapatite.[8] The mineral is also used in cements for bone repair as well as an implant coating for improved biocompatibility and integration of medical devices. At the physiological pH value hydroxyapatite undergoes hydrolysis as follows:

$$Ca_{10}(PO_4)_6(OH)_2 + 12\,H_2O \rightarrow 10\,Ca^{2+} + 6\,H_2PO_4^- + 14\,OH^- \qquad (1)$$

A crack in the bone releases ions into the surrounding solution. The large difference in diffusion coefficients between the cation (Ca^{2+}) and the faster anion (OH^-) [$D(Ca^{2+}) = 0.789\times10^{-5}\,cm^2s^{-1}$, $D(OH^-) = 5.273\times10^{-5}\,cm^2s^{-1}$, $D(H_2PO_4^-) = 0.959\times10^{-5}\,cm^2s^{-1}$] induces a local electric field oriented outwards, away from the crack in the bone surface (i.e., the ion source). Charged moieties introduced in the system respond to this electric field by undergoing diffusiophoretic motion. In an unbounded solution of a symmetrically charged binary electrolyte with a uniform concentration gradient ∇_c, the diffusiophoretic velocity of a charged particle, U, is given by the equation:[9]

$$U = \frac{\varepsilon kT}{Ze\eta}\left[\left(\frac{D^+ - D^-}{D^+ + D^-}\right)\zeta_p - \frac{2kT}{Ze}\ln(1-\gamma^2)\frac{\nabla_c}{c_0}\right] \qquad (2)$$

where D^+ and D^- are the diffusion coefficients of the cation and anion, respectively, Z is the absolute value of the valences of the ions, e is the charge of an electron, k is the Boltzmann constant, T is the absolute temperature, ε is the dielectric permittivity of the solution, η is the viscosity of the solution, ζ_p is the zeta potential of the particle, $\gamma = \tanh(Ze\zeta_p/4kT)$, and c_0 is the bulk concentration of ions at the particle location, as if the particle was not there. Typical electric fields generated in diffusiophoretic systems are 1–10 $V\,cm^{-1}$, sufficient to cause directed motion of charged particles. Electric fields of similar magnitude are also known to cause galvanotaxis of motile cells (reorientation and migration along the direction of the electric field).[2]

In our system, anionic or cationic moieties are expected to respond to the diffusion-induced electric field generated by slow dissolution of hydroxyapatite by moving towards or

[*] V. Yadav, Prof. A. Sen
Department of Chemistry, The Pennsylvania State University
University Park, PA 16802 (USA)
E-mail: asen@psu.edu
Homepage: http://research.chem.psu.edu/axsgroup
J. D. Freedman, Prof. M. Grinstaff
Department of Biomedical Engineering
Chemistry and Pharmacology, Boston University
Boston, MA 02115 (USA)
E-mail: mgrin@bu.edu
Homepage: http://people.bu.edu/mgrin/

[**] The work was supported by Penn State MRSEC funded by the National Science Foundation (DMR-0820404), and Penn State Materials Research Institute Nanofabrication Lab and the National Science Foundation Cooperative Agreement No. ECS-0335765 and by Boston University and the T32 Pharmacology Training grant (5T32M008541-14; J.F.).

Supporting information for this article is available on the WWW under http://dx.doi.org/10.1002/anie.201305759.

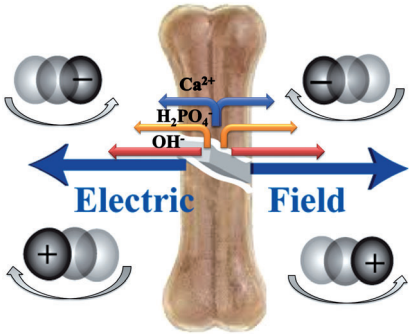

Figure 1. Depiction of the electric field induced by the ion gradient and the resultant particle migration. The lengths of the arrows next to the ions represent their relative mobilities. The generated electric field points outwards away from the crack. Accordingly, the negatively charged particles move towards and positively charged particles move away from the crack.

away from the source (the crack), respectively (Figure 1). To test this hypothesis, we evaluated the mobility of negatively and positively charged quantum dots in the presence of a cracked bone. When the carboxylate-functionalized negatively charged quantum dots were added to a freshly cracked bone within the confines of a hybridization chamber and monitored on a confocal microscope (see the Experimental Section and the Supporting Information for details), the quantum dot intensity was observed to increase within the crack and along its edges owing to the expected diffusiophoretic movement (Figures 2 and 3). In contrast, the amine-

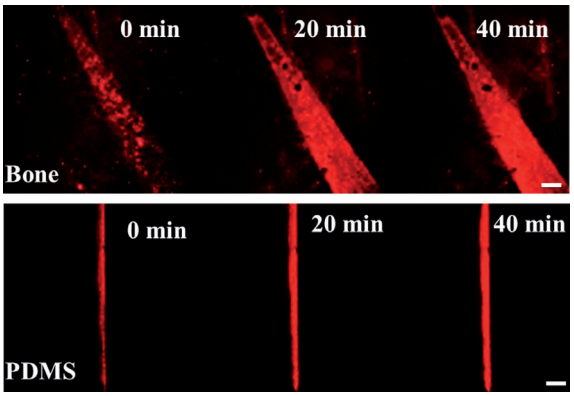

Figure 2. Increasing quantum dot intensity within the crack on bone surface (top) and PDMS surface (bottom) demonstrating an effective damage detection scheme. Scale bar is 60 μm. For confocal images for amine Q-dots and control, see Figure S1 in the Supporting Information.

functionalized, positively-charged quantum dots move outwards, away from the crack (Figure S1a in the Supporting Information). The experiments were carried out in an inverted set-up, eliminating the role of gravity in the quantum dot migration. Control experiments were performed by immersing cracked bone slices in deionized (DI) water for 3–4 weeks, till no further measurable change in conductivity

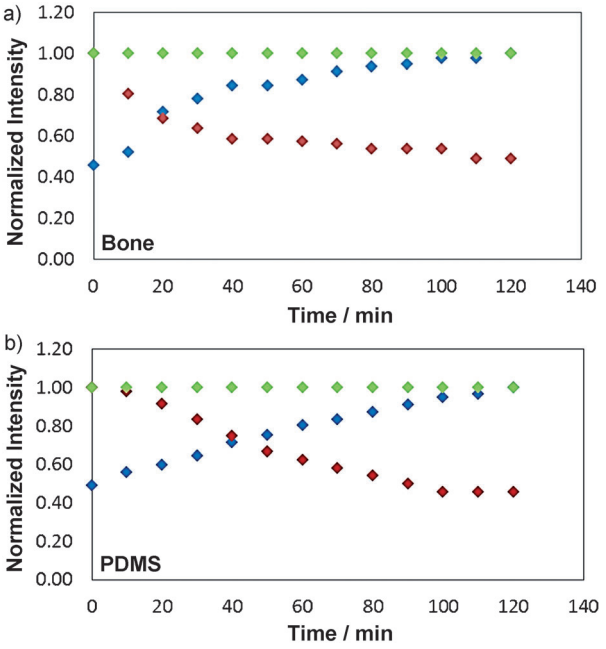

Figure 3. Calculated intensities inside the damage (averaged over the entire damaged area) for HOOC Q-dots (blue), amine Q-dots (red), and control (green) for bone surface (a) and PDMS surface (b). The software Image J was used for analysis.

was recorded after showing an initial increase of approximately 15 $\mu S\,cm^{-1}$ every 10 min. When exposed to quantum dot solution no change in intensity was observed in this case (Figure S1c in the Supporting Information). Marangoni and other nonionic gradient-driven flows can also cause active movement of particles.[10] However, our observation, of opposite directional migration of positively and negatively charged particles, suggests diffusiophoresis to be the dominant propulsion mechanism.

The mechanism described above is not surface-specific, and its versatility can be gauged from its effectiveness on synthetic mineral surfaces as well. To generalize the crack detection mechanism, an artificial system was engineered by embedding hydroxyapatite in between two 1 mm thick polydimethylsiloxane (PDMS) layers. A crack was formed in this "artificial bone" by using a scalpel, and a similar quantum dot migration study was performed. As expected, the negatively charged quantum dots migrated towards the crack, as indicated by the increase in fluorescence intensity (Figures 2 and 3), while the positively charged ones migrated away from the crack (Figure S1b in the Supporting Information). Note that the rate of ion release in solution is governed by the level of hydroxyapatite incorporation and the hydrophobicity of the PDMS. Control experiments with a PDMS layer containing no mineral showed no increase in the quantum dot intensity within the crack over similar time periods (2 h; Figure S1d in the Supporting Information). These data establish an effective and versatile crack detection system utilizing electric fields induced by ion gradients. In principle, any underlying layer of mineral can be effectively utilized to detect cracks on a surface, as long as the cation and the anion have significantly different diffusivities.

To further demonstrate the generality and applicability of this approach, we evaluated the migration of an anionic enzyme to the bone crack site. The enzyme urease was chosen, since it has an isoelectric point below the physiological pH value. Urease was tagged with Dylight melamide 550 in PBS buffer (1 mM; see the Experimental Section for details), introduced over the cracked bone surface, and followed under a confocal microscope. Urease was observed to consistently move towards the crack, thereby increasing the dye intensity within the crack and at its edges. To further support this finding, Raman data were acquired on the enzyme-containing bone samples. Control spectra were collected for both the enzyme and the bone individually and overlaid with the bone sample with the deposited enzyme (Figure 4a). Raman spectra were acquired using a confocal

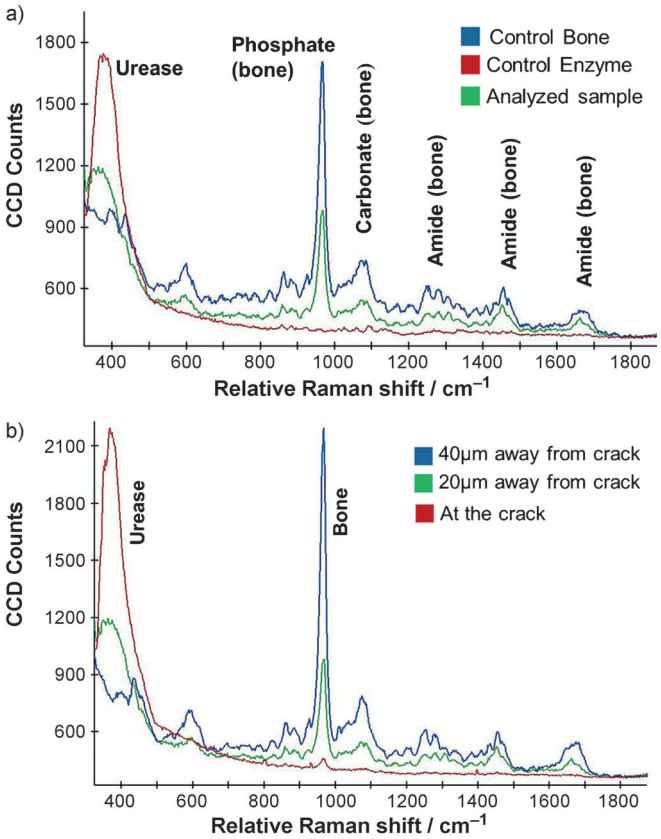

Figure 4. a) Raman spectra obtained on the bone and enzyme separately, overlaid with one collected on the bone exposed to the enzyme. b) Raman spectra at increasing distances from the crack depicting the preferential enzyme migration towards the crack.

Raman microscope equipped with a 40X (NA = 0.6) objective, utilizing a 785 nm diode laser for excitation. The characteristic stokes lines for the human bone can be identified at 965, 1075, and 1269; 1456; 1669 cm^{-1}, indicating the presence of phosphate, carbonate, and amide bonds, respectively (other notable peaks at 862, 596, and 436 cm^{-1}).[11] Urease shows a broad peak centered around 379 cm^{-1}. The presence of these characteristic peaks from both the bone and the enzyme can be noted in the analyzed sample, thus indicating the presence of enzyme at the crack site (Figure 4a).

Conclusive evidence of the enzyme migration towards the crack site was noted upon collection of Raman spectra at increasing distances away from it. Spectra recorded at the precise crack site display an intense enzyme peak along with a noticeable characteristic bone peak (phosphate). As we move away from the crack (in 20 μm steps), the ratio of the characteristic urease peak to that of bone consistently decreases, thereby indicating the diffusiophoretic motion of the anionic enzyme towards the ion source (crack; Figure 4b).

The motion of this self-propelled system was next explored as a targeting mechanism, such as a drug delivery vehicle, transporting biomaterials to the bone-crack site. We prepared negatively charged, fluorescently labeled poly(lactic-co-glycolic acid) (PLGA) nanoparticles containing sodium alendronate (DLS, effective diameter, ca. 220 nm; zeta potential, (24.5 ± 1.1) mV; see the Experimental Section and the Supporting Information for details). PLGA is a well-known biocompatible polymer used in medical devices,[12] and sodium alendronate is a bisphosphonate drug used for the clinical treatment of osteoporosis. The experiments were all performed at the physiological pH value in PBS (1 mM) and followed by using confocal microscopy. Once again increased fluorescence intensity in the crack indicated the active migration of the negatively charged drug-loaded nanoparticles towards the crack (Figure 5).

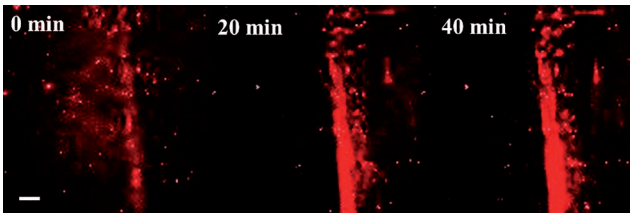

Figure 5. Increasing fluorescence intensity within the crack indicates active migration of drug-loaded PLGA particles tagged with Nile red to the crack site demonstrating an effective drug delivery method. Scale bar is 100 μm.

To confirm that this drug delivery vehicle is indeed capable of delivering an active agent, we performed an in vitro cell proliferation assay[13] (MTS assay, see the Experimental Section for details) with human MG-63 cells, which is an immortalized osteoblast cell line. The colorimetric assay measures an increase in cell proliferation induced by the drug, signified by an increase in optical density. Data is expressed as the percentage of optical density relative to medium alone (control), which is taken as 100% (Figure 6). An increase in cell density was observed in cells treated with alendronate compared to the control (nontreated group), thus demonstrating increased cell proliferation and successful release of the drug from the PLGA nanoparticles. The increased cell growth (ca. 10%) is consistent with other reports[13] and the clinical use of alendronate for bone regeneration and repair.

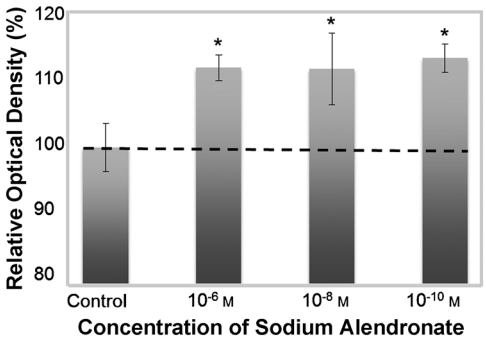

Figure 6. Proliferation of MG-63 cells treated with PLGA nanoparticles containing 10^{-6}, 10^{-8}, and 10^{-10} M alendronate for 48 h, expressed as percentage optical density relative to the negative control of 100%, using a colorimetric MTS cell proliferation assay. (Graph expressed as mean ± standard deviation; significance ($*P < 0.05$), one way ANOVA, Tukey's test, compared with negative control group (medium alone)).

In conclusion, we have described an active, self-propelled particle-based bone crack detection, drug delivery, and repair strategy that requires no external trigger or fuel supply, and is based on ion gradients. This diffusiophoretic mechanism is applicable to a variety of surfaces both biological and synthetic. In our study, the data collected in the presence of a cracked bone were obtained in vitro in PBS buffer at physiological pH value. The use of ion gradients is a new approach to targeting a biological structure that augments current methods that are focused primarily on biomacromolecular interactions involving small molecules, proteins, and nucleic acids. The present work firmly establishes the validity of our approach and calls for a follow-up study.

Experimental Section

Monitoring migration using confocal microscopy: In a typical experiment, the fluorescent solution was introduced into the 9 mm diameter, 0.6 mm thick CoverWell imaging spacer, covering the cracked bone/PDMS samples. The setup was sealed, inverted, and placed on the confocal microscope stage. The fluorescence intensity was monitored at the crack with a 10× objective every 10 min for 2 h after the time taken to set up the experiment (ca. 5 min). $t = 0$ is defined as the point of initial observation.

Fluorescence labeling of urease: Urease (type C-3; Sigma–Aldrich) was tagged with a thiol-reactive dye, Dylight 550 (ex/em: 557/572; Thermo Fisher Scientific). The reaction of the fluorescence probe (40 μM) with urease (2 μM) was carried out in phosphate buffer (150 mM, pH 7) at room temperature for 4–5 h under gentle stirring. The enzyme–dye complexes were further purified using membrane dialysis (10 kDa pores; Amicon ultra-4 centrifugal filter unit, Millipore) to reduce free-dye concentration. The number of dye molecules per catalase enzyme molecule was approximately 2 as quantified by using UV/Vis spectroscopy.

Human bone samples: Bone from human tibia and femur were cut using an IsoMet 3000 (Beuhler, IL) with a diamond metal bonded, wafering blade. Samples were cut at approximately 500 micrometer thickness at low speed using a saline lubrication bath. Bone samples were stored at 4°C in saline and washed with DI water prior to analysis.

Alendronate nanoparticle synthesis and calculation of the drug load:

Synthesis: The drug-loaded nanoparticles were synthesized by adding alendronate sodium (50 mg) dissolved in DI water (1 mL) to a mixture of PLGA (200 mg; MW, 44k) and Nile red (1 mg) dissolved in dichloromethane (5 mL) followed by sonication of the combined mixture for 2 min. A sodium dodecyl sulfate (SDS) solution (20 mL of 0.05 g mL^{-1}) was added and again sonicated for 2 min. After sonication, DI water (100 mL) was added, and the solution was allowed to stir overnight, exposed to air to allow evaporation of the organic solvent. The solution was centrifuged and the resulting pellet resuspended in DI water (5 mL) and centrifuged again. Next, the pellet was resuspended in PBS (1 mM) for analysis and use.

Drug load: The alendronate concentration was determined by a fluorimetric assay of its complex with fluorescamine. The PLGA nanoparticles were degraded in sodium hydroxide solution (1M) for 1 h and then the solution was neutralized with hydrochloric acid (1M). Alendronate was reacted with fluorescamine in a pH 10 borate buffer. The fluorescence was compared to that of known concentrations of alendronate to determine the loading.[12,14] The drug loading of the particles was found to be (70.3 ± 5.3)%.

MG-63 cell culture: MG-63 cells (American Type Culture Collection, Manassas, VA) were maintained in Dulbecco's modified Eagle media supplemented with 10% bovine calf serum and 1% penicillin/streptomycin. Cells were maintained in a humidified atmosphere at 37°C and 5% CO_2.[13]

MTS colorimetric assay: MG-63 cells were plated at a density of 1×10^4 cells/well in 96-well plates. After overnight incubation at 37°C, the media was replaced with media/PLGA nanoparticle suspension containing 10^{-6}, 10^{-8}, or 10^{-10} M sodium alendronate and the cells were allowed to incubate for 48 h. Cell viability was tested by using a colorimetric MTS (3-(4,5-dimethylthiazol-2-yl)-5-(3-carboxymethoxyphenyl)-2-(4-sulfophenyl)-2*H*-tetrazolium) cell proliferation assay and absorbance read at 490 nm. Data is expressed as the percentage of optical density relative to medium alone of 100%.[13]

Received: July 3, 2013
Published online: August 26, 2013

Keywords: bone repair · diffusiophoresis · micropumps · nanotechnology · quantum dots

[1] a) G. A. Ozin, I. Manners, S. Fournier-Bidoz, A. Arsenault, *Adv. Mater.* **2005**, *17*, 3011–3018; b) W. F. Paxton, T. E. Mallouk, A. Sen, *Chem. Eur. J.* **2005**, *11*, 6462–6470; c) W. F. Paxton, S. Sundararajan, T. E. Mallouk, A. Sen, *Angew. Chem.* **2006**, *118*, 5546–5556; *Angew. Chem. Int. Ed.* **2006**, *45*, 5420–5429; d) J. Wang, *ACS Nano* **2009**, *3*, 4–9; e) S. Sánchez, M. Pumera, *Chem. Asian J.* **2009**, *4*, 1402–1410; f) Y. Hong, D. Velegol, N. Chaturvedi, A. Sen, *Phys. Chem. Chem. Phys.* **2010**, *12*, 1423–1425; g) J. Wang, K. M. Manesh, *Small* **2010**, *6*, 338–345; h) T. Mirkovic, N. S. Zacharia, G. D. Scholes, G. A. Ozin, *Small* **2010**, *6*, 159–167; i) Y. Mei, A. A. Solovev, S. Sanchez, O. G. Schmidt, *Chem. Soc. Rev.* **2011**, *40*, 2109–2119; j) V. Yadav, H. Zhang, R. A. Pavlick, A. Sen, *J. Am. Chem. Soc.* **2012**, *134*, 15688–15691; k) S. Sengupta, M. E. Ibele, A. Sen, *Angew. Chem.* **2012**, *124*, 8560–8571; *Angew. Chem. Int. Ed.* **2012**, *51*, 8434–8445; l) D. Patra, S. Sengupta, W. Duan, H. Zhang, R. A. Pavlick, A. Sen, *Nanoscale* **2013**, *5*, 1273–1283; m) S. Sengupta, K. K. Dey, H. S. Muddana, T. Tabouillot, M. Ibele, P. J. Butler, A. Sen, *J. Am. Chem. Soc.* **2013**, *135*, 1406–1414.

[2] G. M. Allen, A. Mogilner, J. A. Theriot, *Curr. Biol.* **2013**, *23*, 560–568.

[3] a) S. Arns, R. Gibe, A. Moreau, M. Monzur Morshed, R. N. Young, *Bioorg. Med. Chem.* **2012**, *20*, 2131–2140; b) R. L. Fleurence, C. P. Iglesias, J. M. Johnson, *PharmacoEconomics*

2007, *25*, 913 – 933; c) W. P. Olszynski, K. S. Davison, *Expert Opin. Pharmacother.* **2008**, *9*, 491 – 498; d) D. Wang, S. C. Miller, P. Kopeckova, J. Kopecek, *Adv. Drug Delivery Rev.* **2005**, *57*, 1049 – 1076; e) G. Zhang et al., *Nat. Med.* **2012**, *18*, 307 – 314.
[4] R. G. Russell et al., *Ann. N. Y. Acad. Sci.* **2007**, *1117*, 209 – 257.
[5] A. V. Uihlein, B. Z. Leder, *Endocrinol. Metab. Clin. North Am.* **2012**, *41*, 507 – 525.
[6] C. S. Colón-Emeric, *J. Am. Med. Assoc.* **2006**, *296*, 2968 – 2969.
[7] T. Luhmann, O. Germershaus, J. Groll, L. Meinel, *J. Controlled Release* **2012**, *161*, 198 – 213.
[8] A. Boskey, N. Pleshko Camacho, *Biomaterials* **2007**, *28*, 2465 – 2478.
[9] J. L. Anderson, *Annu. Rev. Fluid Mech.* **1989**, *21*, 61 – 99.
[10] G. Zhao, E. J. E. Stuart, M. Pumera, *Phys. Chem. Chem. Phys.* **2011**, *13*, 12755 – 12757.
[11] R. Smith, I. Rehman, *J. Mater. Sci. Mater. Med.* **1995**, *5*, 775 – 778.
[12] E. Cohen-Sela, M. Chorny, N. Koroukhov, H. D. Danenberg, G. Golomb, *J. Controlled Release* **2009**, *133*, 90 – 95.
[13] Y. Xiong, H. J. Yang, J. Feng, Z. L. Shi, L. D. Wu, *J. Int. Med. Res.* **2009**, *37*, 409 – 416.
[14] O. Ullrich, T. Reinheckel, N. Sitte, R. Hass, T. Grune, K. J. Davies, *Proc. Natl. Acad. Sci. USA* **1999**, *96*, 6223 – 6228.

